

2021-12-01

Global Analysis of the Hydrologic Sensitivity to Climate Variability

Marisol Dominguez
University of Texas at El Paso

Follow this and additional works at: https://scholarworks.utep.edu/open_etd



Part of the [Environmental Sciences Commons](#), [Geology Commons](#), and the [Hydrology Commons](#)

Recommended Citation

Dominguez, Marisol, "Global Analysis of the Hydrologic Sensitivity to Climate Variability" (2021). *Open Access Theses & Dissertations*. 3403.

https://scholarworks.utep.edu/open_etd/3403

This is brought to you for free and open access by ScholarWorks@UTEP. It has been accepted for inclusion in Open Access Theses & Dissertations by an authorized administrator of ScholarWorks@UTEP. For more information, please contact lweber@utep.edu.

GLOBAL ANALYSIS OF THE HYDROLOGIC SENSITIVITY TO CLIMATE
VARIABILITY

MARISOL DOMINGUEZ TUDA

Master's Program in Geological Sciences

APPROVED:

Hugo Gutiérrez-Jurado, Ph.D., Chair

Diane Doser, Ph.D.

Christopher Brown, Ph.D.

Stephen L. Crites Jr, Ph.D.
Dean of Graduate School

Copyright ©

by

Marisol Dominguez Tuda

December 2021

GLOBAL ANALYSIS OF THE HYDROLOGIC SENSITIVITY TO CLIMATE
VARIABILITY

by

MARISOL DOMINGUEZ TUDA, B.S.

THESIS

Presented to the Faculty of the Graduate School of

The University of Texas at El Paso

in Partial Fulfillment

of the Requirements

for the Degree of

MASTER OF SCIENCE

Department of Earth, Environmental & Resource Sciences

THE UNIVERSITY OF TEXAS AT EL PASO

December 2021

Acknowledgements

I would like to express my sincere gratitude to my project advisor, Dr. Hugo Gutierrez-Jurado, for his patience and guidance throughout the completion of this work. Also, for his encouragement to work on different projects allowing me to travel to places around the globe to present this art piece. To my committee members, Dr. Diane Doser and Christopher Brown for being part of this journey while providing their outstanding support and feedback. To the Earth, Environmental, and Resource Sciences department for providing all the elements needed to complete my research project. Most importantly, thanks to God, my family and friends who made this possible. Also, to Hatsumi, my akita-inu, for her everlasting loyalty. Support for the research was provided by NSF Graduate Research Fellowship Award Fellow ID: Fellow ID: 2018252939 Grant # 1848741.

Abstract

Identifying the regions with greatest changes in their hydrologic behavior under extreme weather events in the 21st century, constitutes a study priority of global impact. Here, we present a global assessment assessing the sensitivity of the world's water landscapes to climate variability during 2001-2016, using a new metric called the Hydrologic Sensitivity Index (HSi). This equation is based on the well-known Budyko curve that uses annual values of Potential and Actual Evapotranspiration (PET and AET), and Precipitation (P), to assess the hydrologic behavior of a location under a given climatic condition by plotting the Evaporative Index (AET/P) against the Dryness Index (PET/P). For values $HSi \geq 1$: Sensitive and $HSi < 1$: Resilient. Also, since elevation, slope and aspect are the three of the defining factors in temperature and humidity regimes, we evaluate their influence on HSi. Overall, majority of the world's biomes display tendency toward drier state. Particularly, we identify the regions with hydrologic sensitivity to climate variability in tropical rainforests accompanied with decreasing water yields and warmer/drier conditions evident along southernmost part of Amazon and central part of the Congo basin. High sensitivity is also seen along easternmost Canadian and Eurasian arctic tundra and boreal forests with increasing water yield trends and dominant warmer/drier climate conditions. The hydrologic sensitivity is amplified at high elevations and steep-sloped terrain outlining the importance of the topography in modulating these effects. We direct the attention towards climate warming resulting in decreased forest cover as potential mechanism driving the decreasing water yield patterns in tropical zones, while snow melt and increasing precipitation in the tundra and boreal forests resulting in surplus water yields. Our global study highlights the particular locations with greatest hydrologic changes to climate variability while outlining the main water yield and climate directions—a study that indicates where water resources have been changing the greatest and in what ways.

Table of Contents

Acknowledgements.....	iv
Abstract	v
Table of Contents.....	vi
List of Tables.....	vii
List of Figures.....	viii
Chapter 1: Introduction	1
1.1 Background.....	1
1.2 Concept of Elasticity	2
1.3 Novelty of this global assesment.....	3
Chapter 2: Methods.....	5
2.1 Data Collection.....	5
2.2 A new metric: Hydrologic Sensitivity Index	6
2.3 Computing HSi.....	8
2.4 Computing Mean Sensitive Area	9
2.5 Computing the effect of elevation, slope, and aspect.....	12
Chapter 3: Results.....	13
3.1 Average annual excess water used from storage (y_0) (i.e., groundwater-dependent ecosystems).....	13
3.2 Frequency HSi.....	14
3.3 Mean sensitive area per biome w/climate and water yield direction.....	18
3.4 Water yield and climate direction for regions with high HSi frequency	19
3.5 Effect of topographic parameters on HSi	21
Chapter 4: Discussion	24
4. Discussion.....	24
Chapter 5: Conclusions	27

List of Tables

Table 1: Data Collection	6
---------------------------------------	---

List of Figures

Figure 1: Budyko’s Framework.....	3
Figure 2: Adapted Budyko Curve.....	7
Figure 3: HSi Algorithm.	9
Figure 4 : Mean Hydrologic Sensitive Area Concept.....	11
Figure 5: Global Terrestrial Ecosystems.....	11
Figure 6: Global Map: Average annual excess water used from storage	13
Figure 7: Frequency of Hydrologic Sensitivity	14
Figure 8a: Coefficient of Variation of Dryness Index	15
Figure 8b: Coefficient of Variation of Evaporative Index	15
Figure 9: Hydrologic Sensitive Area	17
Figure 10: Water yield direction of Hydrologic Sensitive Regions	18
Figure 11: Climate direction of Hydrologic Sensitive Regions	18
Figure 12: Frequency HSi at varying values of elevation, slope, and aspect.....	21

Chapter 1: Introduction

1.1 Background

Global warming and human interventions are changing the behavior of Earth's water cycle (Stott, 2016, Easterling et al., 2017, Sterling et al., 2013, Rodell et al., 2018, Tabari, 2020). Although there is evidence that extreme weather events and increasing climatic variability are intensifying hydrologic processes worldwide (Held & Soden, 2006, Milly et al., 2015, Huntington, 2006, Tabari, 2020, Creed et al., 2014), there is still no consensus on the direction or the magnitude in which different components of the water cycle will respond in the world's major terrestrial ecosystems under these imposed changes (Stott, 2016, Zhan et al., 2012, Salmoral et al., 2015, Martens et al., 2018, Padron et al., 2017). As the current human population arrives at a critical environmental carrying capacity, and the world enters a warmer climate, our planet's ecosystems are changing and adapting (Seddon et al., 2016, Pecl et al., 2017), bringing along changes in the way water is partitioned in the landscape (Milly et al., 2005; Held & Soden, 2006; Huntington 2006; Creed et al., 2014; Tabari, 2020). Whether natural or human induced, ecosystems' alterations to the water cycle at the global scale need to be urgently assessed. Particularly in the face of increasing climate variability and the rising numbers and intensity of extreme weather events altering hydrologic processes worldwide (Stott, 2016; Milly et al., 2005; Zhan et al., 2012). Thus, looking at variations in hydrologic response as a function of the variability in climatic forcing offers an opportunity to detect regions where hydrologic dynamics are changing (Gao et al., 2016). Furthermore, identifying locations with changing hydrologic responses to climatic variability is important for detecting regions arriving at critical thresholds that may compromise the availability of water for both ecosystems and human settlements.

1.2 Concept of Elasticity

Assessing the hydrologic sensitivity to climate variability can be approached from the concept of elasticity. Elasticity here is defined as the capacity of a system to keep a consistent response in spite of sudden perturbations, and/or extreme climatic variability (i.e. hydrologic resilience; Creed et al., 2014). Thus, in that sense, hydrologic sensitivity is the inverse of elasticity, and can be used to detect regions with unstable hydrologic systems. The elasticity concept has been devised using the well-known and widely used Budyko's curve (Creed et al., 2014, Roderick et al., 2014, Helman et al., 2017, Sinha et al., 2018, Padron et al., 2017), which provides a reference condition on the behavior of the long term mean water balance as a function of the average climatic condition of an area (Trenberth, 2011, Roderick et al., 2014, Helman et al., 2017, Li et al., 2019, Budyko, 1974, Greve et al., 2016) (Figure 1). It uses annual values of Potential and Actual Evapotranspiration (PET and AET respectively), and Precipitation (P) and examines changes in the Evaporative Index (i.e. hydrologic response, $EI = AET/P$) against changes in the Dryness Index (i.e. climate condition, $DI = PET/P$) over defined periods of time. Simply put, Budyko's curve represents the historical average of multiple catchments across varying climate types. Therefore, a region's EI can be obtained along the curve given information on its climate (DI). Thus, elasticity (e) is quantified by how far the EI deviates from the Budyko's curve relative to the change in DI defined as the ratio between the range of the dryness index (ΔDI) and that of the evaporative index relative to the curve (ΔEI_R) (Creed et al., 2014) (Equation 1). Positive deviation ($+\Delta EI$, more AET) indicates less water yield ($-Q$, water left over on Earth's surface after evaporation has taken place) while negative deviation ($-\Delta EI$, less AET) indicates greater water yield ($+Q$) (Figure 1). A catchment has high elasticity when there is a small deviation in EI_R relative to change in DI ($e > 1 = \Delta DI > \Delta EI_R$, resilient) and low elasticity when a great deviation of EI_R occurs relative to DI ($e < 1 = \Delta DI < \Delta EI_R$, sensitive).

$$e = \frac{\Delta DI}{\Delta EI_R} = \frac{\Delta DI}{\Delta(EI-B)} \quad (1)$$

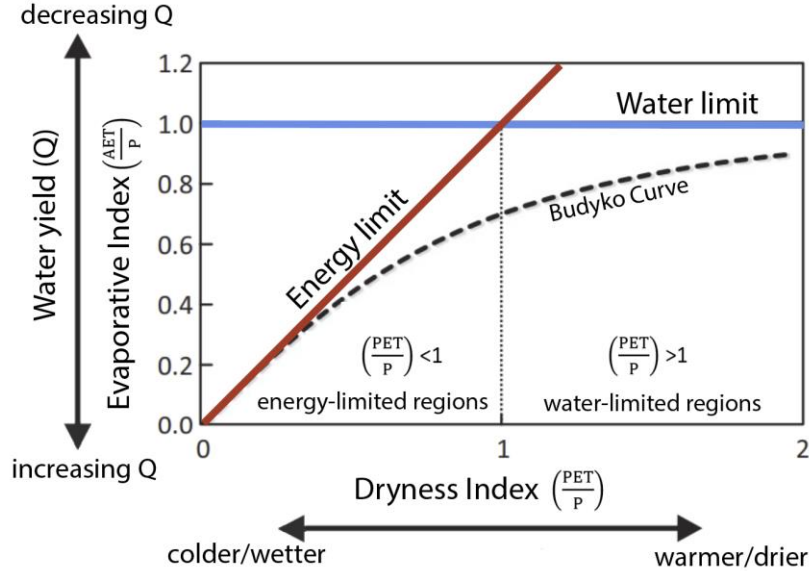


Figure 1: Budyko's Framework. The framework plots the evaporative index against the dryness index. When the evaporative index increases (decreases) the water yield decreases (increases). The solid lines represent the energy (red) and water limit (blue) lines, and the dashed line represents the historical average of where regions would plot given information on their climate (known as the original Budyko curve) (Creed et al., 2014, Budyko, 1974).

1.3 Novelty of this global assesment

Although previous studies have documented regions undergoing hydrological changes using the concept of elasticity for showing how varying climate and the intensification of human activities can have a strong influence on year-to-year changes in hydrologic responses, (Wu et al, 2017b, Creed et al., 2014, Helman, 2017, Li et al., 2019, Wu et al., 2017), they have only been assessed in a few catchments within geographically limited regions. Because of this limited geographic extent, other important factors known to modulate climatic variability, such as elevation, slope and aspect, have been obviated. For example, elevation and aspect in complex terrain alter temperature and humidity regimes across different land conditions within similar climatic zones. Elevation leads to changes in temperature and precipitation regimes which are further amplified by slope and aspect creating distinct microclimates (Gutiérrez-Jurado et al.,

2006, Sristava et al., 2020). Together, these factors influence the partitioning of water in the landscape and hence its hydrologic response over time (Gutiérrez-Jurado et al., 2007), raising questions about which of them plays a major role in maintaining a consistent hydrologic behavior in spite of large climatic perturbations (e.g. climatic deviations from the normal). Changes to hydrologic functioning in response to climatic perturbations are expected to vary widely according to land cover conditions, topographic complexity of the terrain and geographic location (Sterling et al., 2013), specifically in places where sensitive characteristics to these perturbations are relevant. Thus, it is important to evaluate the hydrologic responses to climatic variability globally, and to assess the recurrence (frequency) of heightened responses, while evaluating the role of terrain properties in locations where relatively minor perturbations result in significant changes in hydrologic functioning.

In this study, we evaluate the hydrologic responses to climatic variability globally, and assess the frequency of these responses, while evaluating the role of major topographic factors in modulating these responses. Given that different biomes (climate types) have unique characteristics and the way they respond to extreme climate forcing is inextricably linked to how it will affect water resources (Padron et al., 2017, Motew & Kucharick, 2013, Gudmunsson et al., 2016), we explore the resulting hydrologic sensitive areas for each of the different terrestrial biomes in the world. Finally, we document the average direction in which hydrologic changes occur in these sensitive areas, noting if these regions are shifting to drier (+ Δ DI) or wetter state (- Δ DI) and if they are yielding more (- Δ EI) or less (+ Δ EI) water.

Chapter 2: Methods

2.1 Data Collection

We use annual values of the 3 key variables (AET, PET and P) for the period of January 2001 to December 2016 due to the availability of datasets. The main characteristics (i.e. component, product, temporal resolution, spatial resolution) of the satellite products used are listed in Table 1. AET is derived from Penman Monteith Leuning version 2 (PML-V2) at 500m resolution (Zhang et al., 2019). The PML_V2 product performs well against observations at 95 flux sites across the globe and is similar to or noticeably better than major state-of-the-art AET products such as PML-V1, MOD16, and GLEAM (Zhang et al., 2019). PET is derived from the Moderate-Resolution Imaging Spectroradiometer (MOD16A2) version 6 onboard the Terra satellite and produced at 500m resolution (Running et al., 2019). It has been validated over 46 eddy flux towers, and the close agreement in the seasonality between data reveals the reasonability (magnitude, range and directions of variations) for valid pixels (Running et al., 2019). P is derived from the Multi-Source Weighted-Ensemble Precipitation dataset (MSWEPv2) at 0.1-degree resolution (Beck et al., 2019a). This dataset, MSWEPv2, combines gauge and satellite products, with multiple corrections for regional differences and has shown to be a robust dataset when compared to other P products with a high spatial resolution (Beck et al., 2019b) is ($\leq 0.1^\circ$) which include Climate Hazards Group Infrared Precipitation with Stations (CHIRPS; 0.05°), CPC morphing technique (CMORPH; 0.07°), Global Satellite Mapping of Precipitation (GSMaP; 0.1°), Integrated Multi satellite Retrievals for Global Precipitation Measurement (IMERG; 0.1°), and Precipitation Estimation from Remotely Sensed Information Using Artificial Neural Networks–Cloud Classification System (PERSIANN-CCS; 0.04°). Overall, the three products used in this study have been tested worldwide and span a variety of climates and land

cover types providing the opportunity to apply these datasets for studies of global terrestrial water and energy cycles and environmental changes.

Table 1: Data Collection. List of products with temporal and spatial resolution used to evaluate HSi.

Variable	Product	Temporal resolution	Spatial resolution	Reference
AET (April 4, 2002-present)	PML-V2 (Penman-Monteith-Leuning Version 2)	8-day	500m	Zhang et al.(2019)
PET (2001-present) AET(2001)	MODIS (MOD16A2.006 Modeling Imaging Spectroradiometer)	8-day	500m	https://doi.org/10.5067/MODIS/MOD16A2.006
P (1979-Oct. 2017)	MSWEP-v2 (Multi-Source Weighted Ensemble Precipitation Dataset Version 2)	Daily	0.1° (11,100m)	Beck et al. (2019)
DEM Digital Elevation Models (Elevation, Aspect, & Slope)	SRTM & GTOPO30 (Global 30-arc Second Elevation >60° N) (Shuttle Radar Topographic Mission 90m <60° N)	GTOPO30:1996 SRTM:2008	GTOPO30:1° (~1000m) SRTM: 90m	http://lta.cr.usgs.gov/GTOPO30

2.2 A new metric: Hydrologic Sensitivity Index

This study focuses on identifying regions that are most sensitive or are likely change to an alternative or permanent state in hydrologic functioning. Thus, we developed a new metric called the Hydrologic Sensitivity Index (HSi) by taking the inverse of the elasticity formulation. However, since Budyko’s framework is limited to steady-state conditions (Greve et al., 2016) and this study is executed at interannual scale, the Budyko’s formulation needs an adjustment. Specifically, at sub-annual and interannual timescales, changes in storage water terms such as soil moisture, groundwater, snow storage or human interventions results in $AET > P$ (additional water other than P) does not characterize steady state conditions (Greve et al., 2016). Consequently, we apply the adapted Budyko formulation presented by Greve et al., 2016 to account for changes in storage (B_A) (Equation 2a and Figure 2) using the parameter y_0 , which

represents a measure of the maximum amount of additional water besides P being available to AET (Equation 2b). This parameter is calculated as the difference between AET and P (only when $AET - P > 0$) normalized by PET. The parameter k is a free model constant that can be interpreted as a factor other than the aridity index that influence the water partitioning of EI and was determined to be $\kappa = 2.6$ corresponding to the best fit to the original Budyko function. However, since this parameter varies by region it must be estimated (Greve et al., 2016).

$$B_A = \frac{AET}{P} = 1 + -\frac{PET}{P} \left(1 + (1 - y_0)^{k-1} * \left(\frac{PET}{P} \right)^k \right)^{\frac{1}{k}}, \quad (2a)$$

$$\text{where } y_0 = \frac{AET - P}{PET}, \text{ if } AET - P > 0 \quad (2b)$$

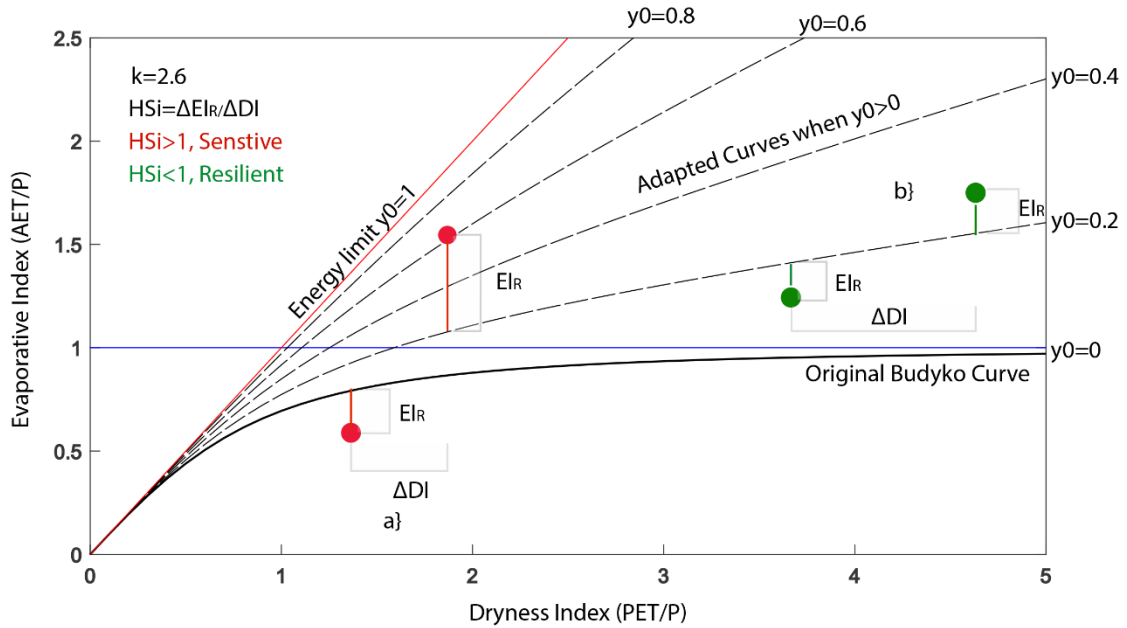


Figure 2: Adapted Budyko Curve. The Budyko framework accounts for changes in storage for regions where $AET - P > 0$, so that the range in EI_R is in reference to the adjusted curve, while range in DI is not affected. HSi is calculated as the ratio of a catchment's range in EI to its range in DI between consecutive pair of years: $HSi = (\Delta DI) / (\Delta EI_R)$, where a) high sensitivity ($HSi > 1$, red) (i.e., approximating theoretical behavior), and b) low hydrologic sensitivity ($HSi < 0$, green) (i.e., deviating from theoretical behavior).

Hence, by tracking the changes in hydrologic response (ΔEI_R) of a location or region relative to the adapted curve (B_A), that is, its water yield deviation to interannual climatic variability (ΔDI) for consecutive years, we can calculate the hydrologic sensitivity in the following manner:

$$HSi = \frac{\Delta EI_R}{\Delta DI} = \left| \frac{\Delta(EI_R - BA)}{\Delta DI} \right|, \quad (3)$$

where sensitive regions will display $HSi > 1$, and resilient locations will show $HSi < 1$ (Equation 3). It is important to note that HSi evaluates the absolute difference between DI and EI_R between successive years, regardless of which year was warmest or wettest. A conceptual diagram depicting the algorithm used is shown in Figure 2, of which a detailed description is provided next. HSi evaluates the absolute ratio between ranges in DI and EI_R values between consecutive years (e.g. $HSi = |\Delta EI_R / \Delta DI| = |\Delta EI_{R,2001-2002} / \Delta DI_{2001-2002}|$).

2.3 Computing HSi

Knowing the year-to-year hydrologic sensitivity is more meaningful when looked over a longer period of time. Regions consistently showing sensitive behavior can be identified by looking at the frequency with which $HSi > 1$ is detected. Figure 3 displays the algorithm for computing HSi frequency. First, we compute annual values of AET, PET, P, and y_0 . Next, we compute HSi for every successive pair of years from 2001 to 2016. All computations leading to the HSi are performed in the Google Earth Engine Platform (Golerick et al., 2017). A total of 15 HSi maps were obtained representing the HSi for each consecutive pair of years. For each map, where $HSi > 1$, regions are classified as *Sensitive* and for $HSi \leq 1$, *Resilient*. To provide a synthesis of the general trend of global hydrologic sensitivity, we display the frequency of HSi , showing the recurrence of $HSi > 1$ for every terrestrial location with a range of 0 (low frequency) to 15 (high frequency). Regions where frequency $HSi \geq 7$ are considered highly recurring and as such are deemed as the most hydrologically sensitive.

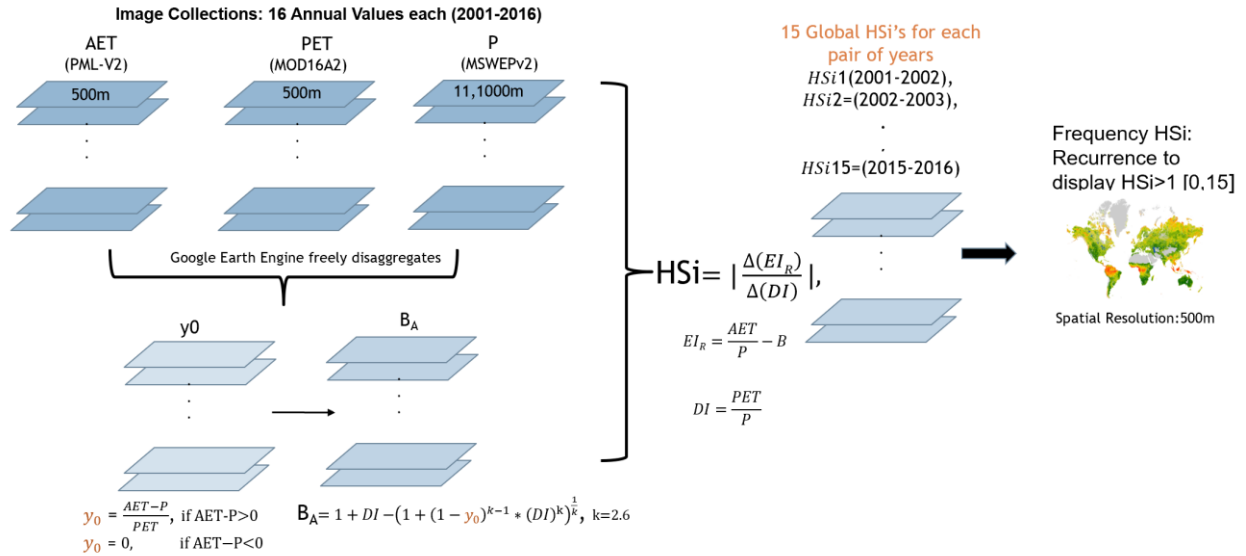


Figure 3: HSi Algorithm. Flowchart for computing HSi. Input data layers are shown in medium blue, intermediate data layers computed in Google Earth Engine as part of the algorithm are shown in light blue, and final output is displayed as a map of HSi Frequency.

2.4 Computing Mean Sensitive Area

Besides the geographic occurrence of hydrologic sensitive areas, identifying the percentage of sensitive area relative to the total area in a biome can help inform the regions of the world where hydrologic response has been consistently changing. Figure 4 displays the algorithm for estimating the mean hydrologic sensitive area for each terrestrial biome. For this analysis, the biome boundaries were obtained from Terrestrial Ecosystems of the World (TEOW) shapefiles (Figure 5) by the World Wildlife Fund (Olson et al., 2001). The 15 pairs of ΔEI_R 's and ΔDI 's per biome are used to quantify sensitive for every consecutive pair of years. Hydrologic sensitive areas are represented by the colored quadrants (green and red or light and dark blue). All colored area shows that the interannual absolute change in evaporative index, $|\Delta EI|$, is greater than the interannual absolute change in the dryness index, $|\Delta DI|$ which is equivalent to $|HSi| > 1$. The diagram is split into 4 quadrants indicating the possible climate and water yield directions: drier (+ ΔDI) wetter (- ΔDI) and less water yield (+ ΔEI) and more water yield (- ΔEI). Sensitive area (grid cells) where $|HSi| > 1 = |\Delta EI_R| > |\Delta DI|$ equivalent to:

I = $\Delta EI_R > \Delta DI$ = less water yield and drier climate;

II = $\Delta EI_R > -\Delta DI$ = less water yield and wetter climate;

III = $-\Delta EI_R < -\Delta DI$ = more water yield and wetter climate;

IV = $\Delta EI_R < \Delta DI$ = more water yield and drier climate.

Sensitive area is defined by the percentage of sensitive grid cells ($HS_i > 1$) to the total number of grid cells within each biome. Once we obtain all 15 values (one per pair of years) of sensitive area per biome, we compute the temporal average. Additionally, we display sensitive areas with direction of change by including the portion of sensitive area allocated toward drier vs wetter climate conditions (Figure 4a) and less vs greater water yield (Figure 4b) and direction of change. For instance, the percentage of sensitive grid values toward warmer/drier (ΔDI) and colder/wetter ($-\Delta DI$) values defines the climate direction, while decreasing (ΔEI) and increasing ($-\Delta EI$) water yield defines the water yield direction. Also, the fraction of the sensitive area is plotted relative to the global land area to provide a global areal extent of sensitivity for each biome. In addition, we created two maps to spatially display the median climate and water yield trends for regions with $HS_i > 1$ and Frequency ≥ 7 .

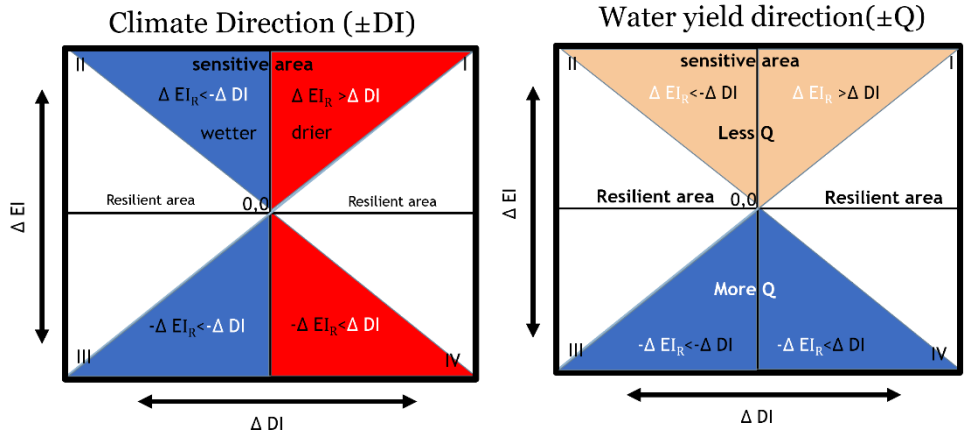


Figure 4 : Mean Hydrologic Sensitive Area Concept. The diagrams show how the hydrologically sensitive area is calculated. **a)** Quadrant I and IV where hydrologic sensitive areas have become drier (red), so that the change in $+\Delta DI$ is positive, while in quadrant II and III represents the areas which have become wetter the absolute change in $-\Delta DI$ is negative (green). **b)** Quadrant I and II represent the condition where hydrologic sensitive areas show decreasing water yield trends, so that the change in $+\Delta EI_R$ is positive (light blue), while in quadrant III and IV represent the areas that show increasing water yield trends, so that the change in $-\Delta EI_R$ is negative (dark blue).

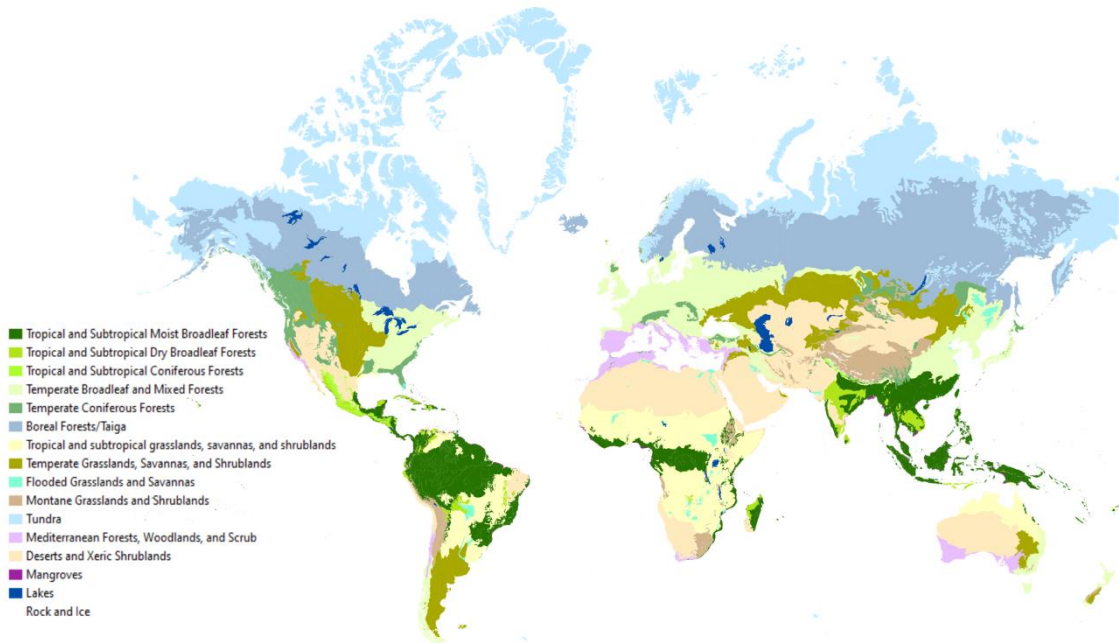


Figure 5: Global Terrestrial Ecosystems. A total of 14 Major Terrestrial Ecosystems reflect the diverse climate types (we do not consider lakes and rock ice biomes for this study). Terrestrial communities represented here include the full extent of continental topographic relief (Oslon, 2001).

2.5 Computing the effect of elevation, slope, and aspect

We evaluate the effect topography on hydrologic sensitivity by plotting the average HSi frequency for all elevations ranges (binned every 100 m), aspects (binned every 22.5°), and slope steepness (binned every 5°) against latitudinal change. For this analysis we used global digital elevation models (DEMS) from the Shuttle Radar Topography Mission (SRTM, Jarvis et al., 2008) data (90 m resolution; version 4, for latitudes < 60° N and GTOPO30 (1° resolution; <http://lta.cr.usgs.gov/GTOPO30>) for latitudes > 60° N as seen in Table 1. Slope and aspect maps were derived from the DEMs using standard GIS-based methods in ArcMap 10.7. (Burrough et al., 2015). The elevation range used is 0 to 7000 meters above sea level (m.a.s.l), aspect (N, NE, E, SE, S, SW, W, NW) specifically above slope values greater than 10° (no flat areas used), and slope 0 to 90 degrees.

Chapter 3: Results

3.1 Average annual excess water used from storage (y_0) (i.e., groundwater-dependent ecosystems)

We note where water storage was used to supplement precipitation to satisfy the annual AET ($y_0 > 0$; Figure 6), except in locations where “no data” values in either AET or PET impeded the calculation of y_0 (gray areas in Figure 6). In particular, high values ($y_0 > 0.2$) occur along the Yucatan Peninsula ($y_0 \sim 0.3-0.4$, Mexico), California ($y_0 \sim 0.30-0.35$, USA) and Great plains ($y_0 \sim 0.25$, USA), Patagonia ($y_0 \sim 0.28-0.41$, Argentina), Tamil Nadu and Rajasthan ($y_0 \sim 0.3-0.4$ India), Caatinga forest ($y_0 \sim 0.26-0.38$, Brazil) and Eastern Africa ($y_0 \sim 0.40-0.65$). Some of these regions showing large y_0 values correspond to groundwater fed irrigated croplands where significant abstraction of water resources subsidizes high AET rates (e.g. Central Valley, California and Central Midwestern USA, Northern India, Northeastern China; Aeschbach-Hertig & Gleeson, 2012). Other areas with large y_0 values show groundwater dependent ecosystems where vegetation has a continual access to water regardless of precipitation conditions yielding high annual AET (e.g. Yucatan Peninsula; Uuh-Sonda et al., 2018). Other regions along the high Arctic tundra, northernmost boreal zones, and equatorial tropical zones display no excess storage ($y_0 \sim 0$), while all other regions have slight excess water storage ($y_0 > 0-0.20$) (see Figure 6).

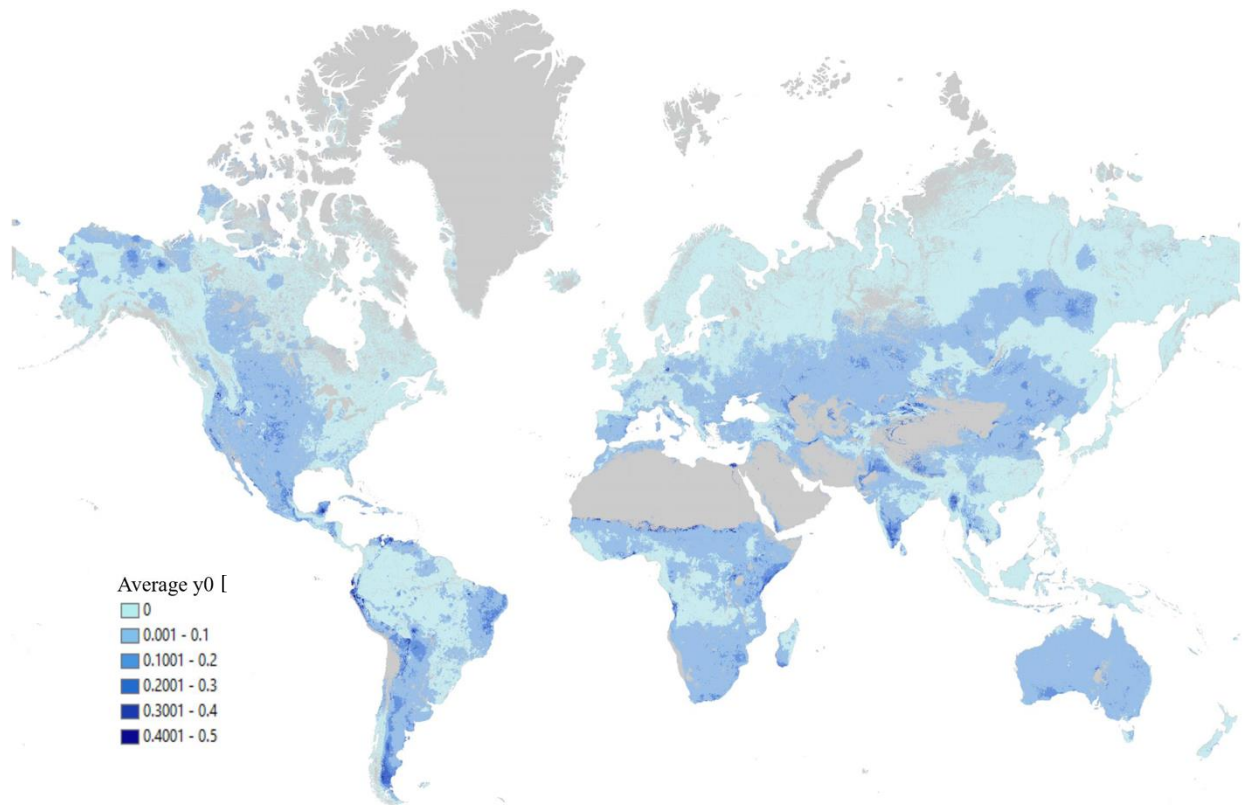


Figure 6: Average excess water used from storage. 16-year average excess water storage as a fraction of the potential evapotranspiration (additional water other than P available to AET standardized by PET). The values range from 0 (no significant changes in storage) to 0.4 or greater (red, high changes in storage). Areas with dominant barren land and permanent ice (no data) are shown in grey. Pixel resolution is 500m. Map created in Google Earth Engine and modified with continental outline shapefile in ArcGIS 10.7 software.

3.2 Frequency HSi

The areas exhibiting the most frequent hydrologic sensitivity during the 2001-2016 period were located in the tropical rainforests (tropical & subtropical moist broadleaf forest) of Central and South America (Amazon Basin), the central-western Africa (Congo Basin), and southeast Asia (Himalayan region, Indochinese Peninsula, and Malay Archipelago), the Arctic tundra, parts of the boreal forest, and tropical and subtropical coniferous forests scattered throughout North America and Eurasia (Figure 7). Overall, arid and semiarid areas worldwide display low frequency (<2) of HSi, and the areas displaying the highest frequency (>7) are in general surrounded by a zone of increasingly lower HSi frequency (orange and yellow areas in Figure 7) outwards.

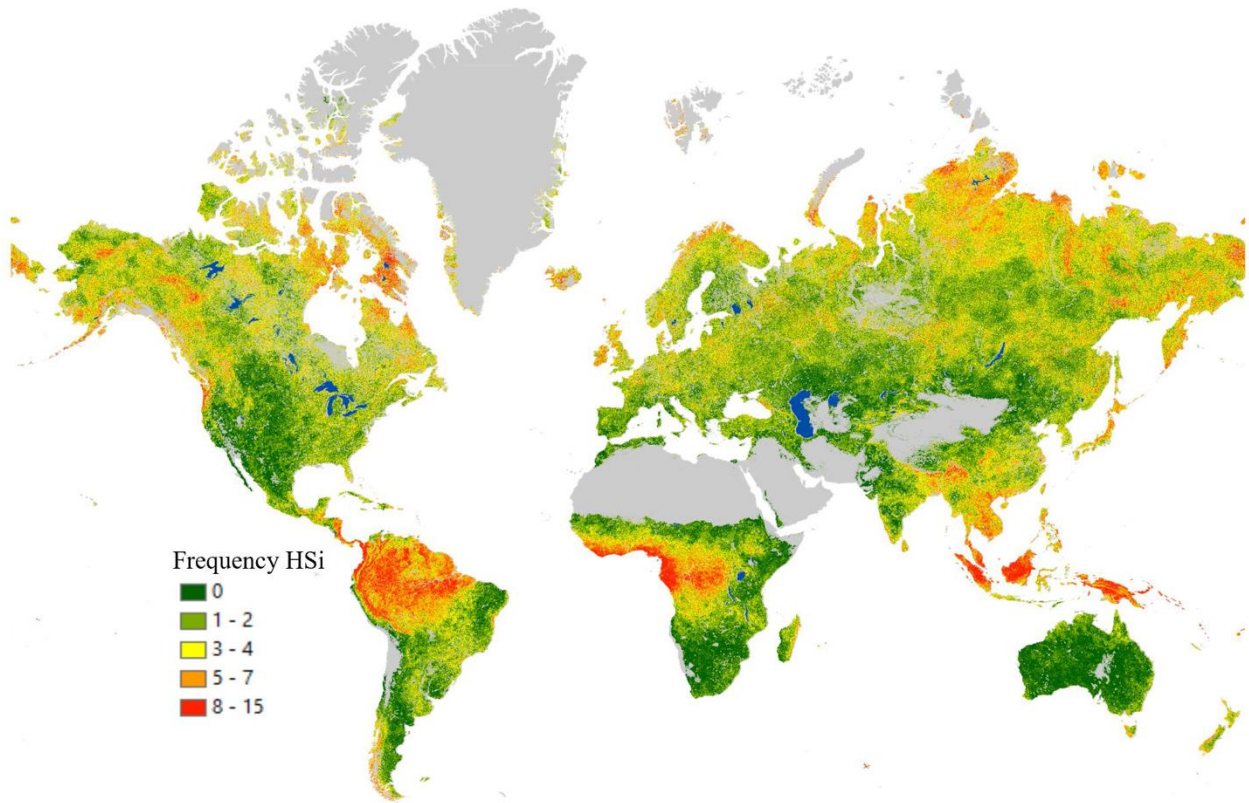


Figure 7: Frequency of Hydrologic Sensitivity. Tendency to high hydrologic response to climate variability (based on the recurrence of $HSi \geq 1$). The index ranges from 0 (no frequency, dark green) to 15 (high frequency, red). Areas with dominant barren land and permanent ice (no data) are shown in grey. Wetland areas, as identified by the Global Lakes and Wetlands Database, are mapped in blue. Pixel resolution, 500m; period, 2001–2016. Map created in Google Earth Engine and modified with continental outline shapefile in ArcGIS 10.7 software

The areas where no hydrologic sensitivity is detected during the period of study (2001-2016) are regions with large interannual variability in climatic conditions. A map showing the coefficient of variation (CV) of the Dryness Index (DI) reveals that the regions of the world where this coefficient is large (values close to 1 show locations with high variability) closely match those with no hydrologic sensitivity (0 frequency of $HSi > 1$; Figure 8.a). In those places the interannual variability of the DI outweighs any moderate or even large variabilities in Evaporative Index (EI; Figure 8.b). By contrast, the areas where the highest frequency of hydrologic sensitivity is observed, correspond to locations with low or moderate interannual variability in DI and EI (i.e. $CV \text{ of DI and EI} < 0.4$). This suggests that hydrologic sensitivity, as measured by HSi, is largely

dependent on the prevailing interannual variability of the fluctuations in climatic conditions expressed by the DI. This finding gives confidence in the ability of the HSi to detect those locations where in spite of having low year to year variations in climatic conditions, relatively large variations in the evaporative index are occurring.

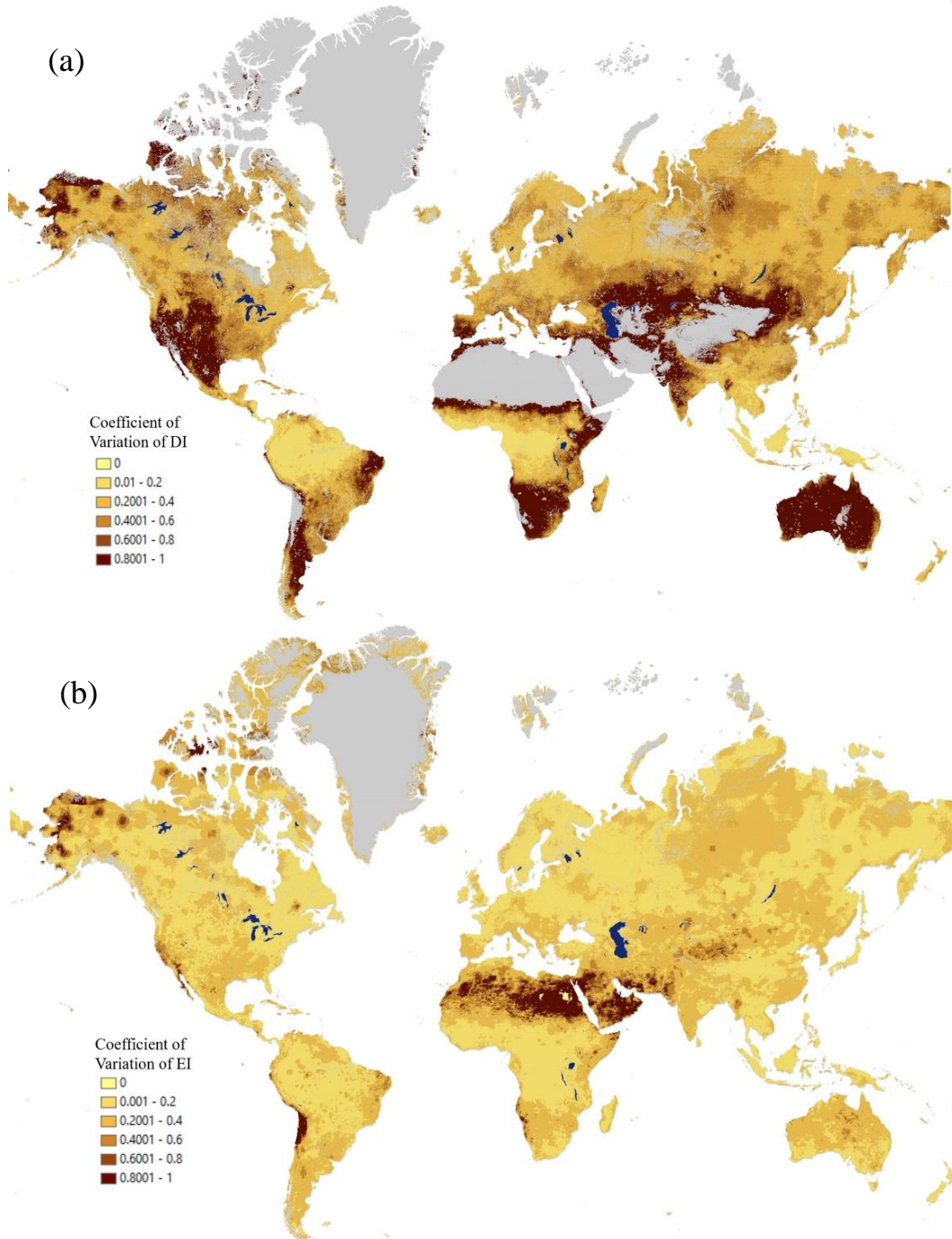


Figure 8. Coefficient of Variation of (a) Dryness Index (DI) and (b) Evaporative Index (EI) for the study period (2001-2016). The coefficient ranges from 0 (low variability, light yellow) to 1 (high variability, red). Areas with dominant sterile soil and permanent ice (no data) are shown in gray. Wetland areas, identified by Global Lakes and Wetlands Database, are mapped in blue. Pixel resolution is 500m. Map created in Google Earth Engine and modified to include continental schema basemap and lakes in ArcGIS 10.7 software.

3.3 Mean sensitive area per biome w/climate and water yield direction

Figure 9 displays mean sensitive area per biome arranged from largest to least hydrologic sensitive. The biomes displaying the largest sensitive area in descending order are tropical rainforests, the Arctic tundra, tropical and subtropical coniferous forests, and boreal forests. Tropical and subtropical rainforests and coniferous forests display decreasing water yields, while tundra and boreal systems display increasing water yields. Relative to global land, boreal forests have the greatest actual areal extent of hydrologic sensitive land followed by tropical rainforests and grasslands (tropical and subtropical grassland, savannas, and shrublands). The hydrologic sensitive area in the majority of the biomes (12 out of 14 biomes) have a clear tendency towards decreasing water yield conditions with the exception of the Arctic tundra and temperate broadleaf mixed forests (mixed forests) which display a neutral behavior. Although the climate direction is roughly neutral for most biomes, the hydrologic sensitive area in 9 out of 14 biomes is slightly inclined toward drier conditions with the exception of the Arctic tundra, mixed forests, temperate coniferous forests, tropical & subtropical coniferous forests, and tropical rainforests, which lean toward wetter/colder conditions.

Hydrologic Sensitive Area per Biome

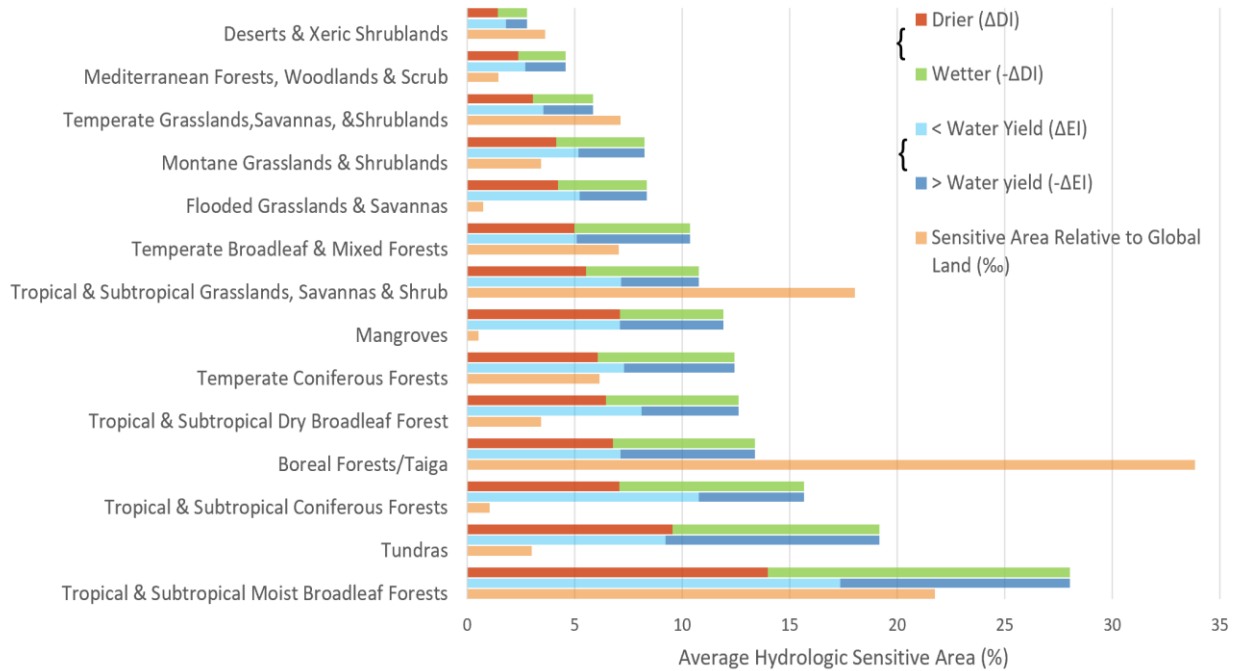


Figure 9: Hydrologic Sensitive Area. Average sensitive area per biome (relative to biome area) with portion indicating direction of change, where drier (red) and wetter (green) conditions refer to the climate direction; less (light blue) and greater water yield (dark blue) refers to the hydrologic direction; average sensitive area relative to the global land area (orange) refers actual extent of sensitivity. Values are computed on Google Earth Engine platform at ~1000m resolution.

3.4 Water yield and climate direction for regions with high HSi frequency

Focusing on only those regions where HSi frequency ≥ 7 (mainly equatorial and northern high latitudes) the median direction in water yield (ΔEI) and climate direction (ΔDI) is displayed in Figure 10 and Figure 11 respectively. In particular, Figure 10 displays dominant decreasing water yield (light orange) for the majority of pixels within tropical forest (equatorial zones) while increasing water yields (blue) are evident in the northern high latitude regions particularly along Alaskan, easternmost Canadian and Eurasian arctic regions and boreal forests. Figure 11 displays a general neutral tendency in climate conditions in dry (red) versus wet (blue) for these same regions. Nonetheless the map displays drying/warmer conditions along southern part of and southern edge of the Amazon basin, western and central Congo Basin and the northeastern part

of the Canadian and Eurasian continent. Colder/wetter conditions are seen along the northern part of the Amazon basin and northmost Siberia.



Figure 10: Water yield direction of hydrologically sensitive regions. For display purposes, observed results are based on median values of interannual change in evaporative index, ΔEI , only for regions where the frequency of $HS_i \geq 7$. The values range from less water yield ($+\Delta EI$, light orange) to greater water yield ($-\Delta EI$, dark blue) conditions. Areas with dominant sterile soil and permanent ice (No Data) and non-sensitive areas are shown in gray. Pixel resolution is 500m. Map created in Google Earth Engine and modified to include continental schema basemap in ArcGIS 10.7 software.

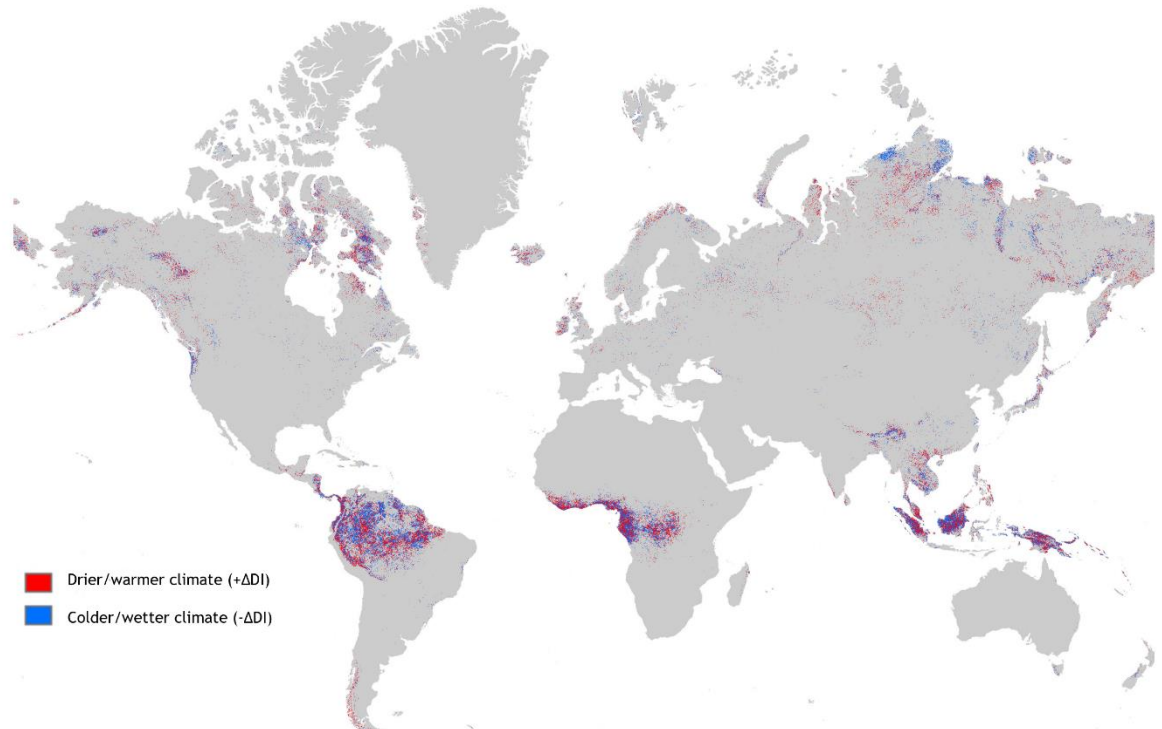


Figure 11: Climatic direction of hydrologically sensitive regions. For displaying purposes observed results are based on median values of interannual change in dryness index, ΔDI , only for regions where the frequency of $HS_i \geq 7$. The index ranges from colder/wetter ($-\Delta DI$, blue) to drier/warmer ($+\Delta DI$, red) climate conditions. Areas with dominant sterile soil and permanent ice (no data) and non-sensitive areas are shown in gray. Pixel resolution is 500m. Map created in Google Earth Engine and modified to include continental schema basemap in ArcGIS 10.7 software.

3.5 Effect of topographic parameters on HSi

The topographic effects on hydrologic sensitive areas are most apparent along high latitude regions, particularly at mountainous locations in both hemispheres, including the Tibetan Plateau ($33^\circ N$) as seen in Figure 12a-c. For example, in Figure 12a elevation appears to be a defining parameter driving hydrologic sensitivity beyond 45° latitude in both the Northern and Southern hemispheres. Conversely, midlatitude regions (between 20° and 40°) in both South and North hemispheres appear to be somewhat hydrologically insensitive to changes in elevation, but most markedly and for a larger latitudinal stretch in the Southern hemisphere. The latitudinal stretch in the Northern Hemisphere where HSi values are low across all elevation ranges is 5° shorter than in the Southern Hemisphere (20° to 40° vs -30° to -45° respectively). Along the

equatorial belt, in between 15° S and 7° N, high HSi values appear at the lowlands (0-500 m.a.s.l) and above ~1500 m.a.s.l throughout all the elevation range, with the highest sensitivity above 2000 m.a.s.l. In the same latitudes, where high HSi is found across elevation gradients, steep slopes (slopes greater than 30°) display high HSi values in Figure 11b, mainly attributed to the various effects of mountainous landscapes that are generally associated with having steep-sloped topography compared to low elevations (Riebe et al., 2015). Along the equatorial zone (~7°N and ~10°S) high HSi values are found at the majority of slope angles but with highest sensitivity at slopes greater than 15°. In the Northern hemisphere, HSi gradually increases beginning at latitude 45° and beyond, but has specific thin latitudinal stretches (~2°) of higher sensitivity at slopes greater than 30° around 50°, 60°, 70° and 80°. In the Southern hemisphere, HSi increases abruptly at higher latitudes beginning at -40° and beyond with highest sensitivity for very steep slopes (slope > 60°). HSi in regions between latitudes of -20° and -40° (location of arid lands) appear to be insensitive at all slope angles and elevations. In our analysis, aspect (orientation of the terrain) did not show an effect on HSi (Figure 12c). This is possibly due to the inability of the HSi data to capture the fine scale microclimatic variability in areas with complex terrain due to the native spatial resolution of the data (>500m). There is evidence that varying aspects in complex terrain modulate the hydrologic response to extreme hydroclimatic events (Gutiérrez-Jurado et al., 2007) and could potentially amplify or mute the HSi of headwater catchments constituting some of the largest inland water yielding areas. Further studies addressing this shortcoming in the analysis with the use of higher resolution data, should provide a clearer picture on the impact of terrain attributes on the HSi of these regions.

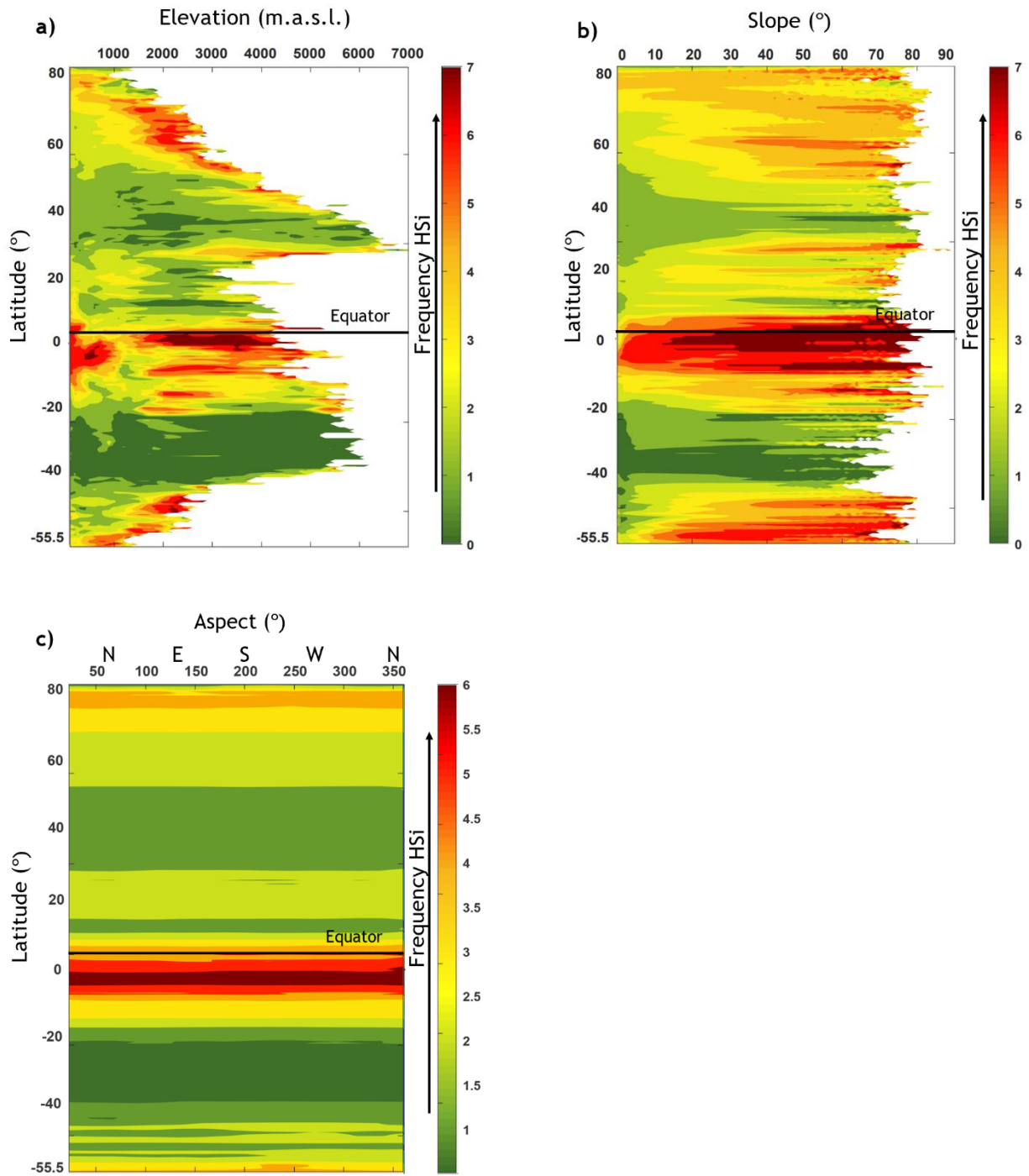


Figure 12: Frequency HSi [0,7+] at varying values of a) elevation [100,7000] in m.a.s.l. b) slope steepness [0,90] in degrees, and c) aspect[0,359] in degrees against latitudinal change from 80N to -55.5S from low frequency (blue) to high frequency (red). Graphs created in MATLAB 2019 software using pixel resolution at 90m for each variable.

Chapter 4: Discussion

4. Discussion

In this study we showed a global map displaying excess storage water. These regions agree with locations of some of the world's groundwater-dependent ecosystems and groundwater-fed irrigated croplands (Rodell et al., 2018, Aeschbach-Herring & Gleeson, 2012). Regions displaying no excess water storage such as northern high latitude regions and equatorial tropical zones are mostly explained by being energy-limited regions and receiving large amounts of precipitation resulting in larger moisture influxes relative to evapotranspiration outfluxes. The relatively simple computation of y_0 can provide a first insight into out-of-water-balance areas that can alter the estimates of hydrologic sensitivity by raising AET totals substantially at the annual scale. Our analyses indicate that the majority of the regions detected as hydrologic sensitive areas are changing towards drier conditions with decreasing water yields. This observation coincides with a phenomenon suggested by Cook et al., (2014), in which vast regions of land in the planet are experiencing at least moderate drying as a warmer climate—generally more able to evaporate moisture from the land surface—in combination with hotter temperatures will favor increasing dryness.

Our results showed that the locations with the highest HSi can be clustered in two regions: (1) tropical zones across all elevation ranges (2) along arctic tundra and boreal zones. For the first region, at equatorial latitudes, we found hydrologic sensitivity in tropical rainforests associated with changing water yields. A majority of tropical regions show decreasing water yields while fewer regions show increasing trends (Figure 8). There is still no consensus as to whether reduced forest cover will increase or decrease water yields across these regions (Bruijnzeel et al., 2004, Zhoue et al., 2013, Roudier et al., 2014, Reyer et al., 2017, Deb et al., 2018). Reduced forest cover, which has been shown to alter precipitation patterns (Ellison et al., 2011, van der Ent et

al., 2010) resulting in reductions in leaf gas exchanges (Seddon et al., 2016, Clark et al., 2003, Staal et al., 2018, Wu et al., 2019) along these regions is a potential explanation to the observed reductions in water yields. Placed in a large-scale context, a great portion of tropical forests' rainfall is water recycled within these basins by forest evapotranspiration (van der Ent et al., 2010, Lenton et al., 2008). For instance, approximately one-third of rainfall in the Amazon (Staal et al., 2018, van der Ent et al., 2010, Lenton et al., 2008), Congo (van der Ent et al., 2010, Dyer et al., 2017), and northern Indonesia and Papua New Guinea basins is regional recycled precipitation (van der Ent et al., 2010). Hence, a reduction in tropical forest cover leads to decreases in forest evapotranspiration which in turn results in reduced precipitation. Consequently, reduced regional recycled precipitation at large scales implies a tendency toward decreasing water yields. This highlights the hydrologic sensitivity of tropical regions to forest cover changes. Continuing deforestation and human land use and disturbances at continental scale, currently highest in this terrestrial biome (Crowther et al., 2015), have the potential to amplify the negative impact observed in water yields (Davidson et al., 2012). In contrast, regions south of Indonesia and Papua New Guinea where ocean moisture is the main precipitation source, show the areas where forest cover loss is accompanied by increasing water yield trends (van der Ent et al., 2010). In addition, there is evidence that regional recycling ratios are amplified in mountainous regions globally since these areas are able to block moisture from entering continents or easily capture moisture from the atmosphere (van der Ent et al., 2010). Accelerating vegetation changes involving biodiversity loss and reduction of tropical alpine areas (Buytaert et al., 2011) is therefore a plausible cause for decreased water yields within these regions.

For the second region, at high latitudes, in the past three decades temperatures have increased rapidly, mainly in the northern hemisphere (Hartmann et al, 2013). As a consequence,

rapid rates of snow melt have been observed in Arctic tundra and boreal forests in response to warming temperatures (López-Moreno et al., 2020, Najafi et al., 2015, Pepin et al., 2015, Myers-Smith et al., 2015, Lamprecht et al., 2015). These regions are warming more rapidly than lower latitudes due to polar amplification of temperature, water vapour, and surface albedo feedbacks (Myers-Smith et al., 2015, Chapin et al., 2005, Hinzman et al., 2013). There is also evidence that this effect is enhanced at high elevation regions where snow accumulation is greatest and changes in precipitation patterns are occurring (e.g. regions in the Tibetan Plateau, Rocky Mountains, Greater Alpine Region) (Pepin et al., 2015, Ohmura, 2012, Zhang et al., 2013, Yan et al., 2016, Palazzi et al., 2019). For example, recent findings have shown increases in lake levels and volumes in the Tibetan Plateau related to temperature amplification resulting in enhanced precipitation from a faster warming rate compared to the mean global warming (Zhang et al., 2020). Also, high latitude and mountainous regions of Siberian and Canadian Arctic and boreal zones have seen increasing water yield trends due to ice-sheet loss, increasing precipitation, thawing and shrub growth in steep slopes (Rodell et al., 2018, Myers-Smith et al., 2015, Zhang et al., 2013). These lines of evidence are consistent with our findings of high HSi areas leaning toward higher water yields in these regions, and particularly those along the Siberian and easternmost Canadian and Eurasian Arctic.

Chapter 5: Conclusions

5. Conclusion

We identified regions with hydrologic sensitivity to climate variability globally and at high spatial and temporal resolution within high and low latitudes. At high latitudes, boreal and arctic zones show heightened hydrologic sensitivity accompanied by increasing water yields, while at low latitudes, tropical rainforests show the largest hydrologic sensitivity with the majority of their sensitive area trending towards decreasing water yields. We found that hydrologic sensitivity is amplified at high elevations and in steep-sloped terrain, outlining the importance of topography in modulating these effects with strong implications for high water yielding headwater catchments. We direct the attention towards climate warming resulting in increasing snow melt and precipitation in Arctic tundra and boreal forests and increasing tree cover loss in tropical forests, as possible mechanisms driving the observed patterns. Although there is no clear consensus yet on the direction surface water yields would take in tropical zones as a result of climate variability, our findings suggest that hydrologic sensitivity may be linked to vegetation changes. Other land cover changes associated with altered climatic patterns across high latitude regions may be contributing to changing hydrologic dynamics (Myers-Smith et al., 2015) in areas displayed in our HSi analysis as highly sensitive locations. Globally, boreal and tropical forests, the two biomes producing the greatest water yields also display the greatest extent of hydrologic sensitive land. This makes them hotspots for hydrologic surveillance of expected impacts from further increases in climatic shifts with the potential to significantly alter the global water cycle. Future work should determine if the hydrologic sensitivity patterns found in this study represent tipping points in changing hydrologic dynamics within each biome, and to assess at the regional and local scale their cascading impacts on ecosystems and human settlements.

Code Availability

Code and datasets used to conduct this analysis are available online from our Google Earth Engine link <https://code.earthengine.google.com/9efbe6a3ccfb488eef80a903d923a30f>. A MATLAB code and associated data to reproduce the topographic analyses is available for download in the following open access repository: <http://doi.org/10.5281/zenodo.4479716>.

Author Information

Marisol Domínguez and Hugo A. Gutiérrez-Jurado: These authors contributed equally to this work.

Marisol Domínguez-Tuda

Present address: Department of Earth, Environmental, and Resource Sciences, University of Texas at El Paso, Texas, United States

Hugo A. Gutiérrez-Jurado

Present address: Department of Earth, Environmental, and Resource Sciences, University of Texas at El Paso, Texas, United States

Contributions

H.A.G. conceived and designed the study. M.D. prepared and processed the data including writing the Google Earth scripts. Both M.D. and H.A.G performed the data analysis, writing and editing of the paper.

Corresponding Author

Correspondence to M. Domínguez and H. A. Gutiérrez-Jurado

Ethics Declaration

The authors declare no competing interests.

Additional Information

Marisol Dominguez, & Hugo A. Gutiérrez-Jurado. (2021). Global dataset for evaluating impact of topographic factors on hydrologic response to climate variability (Version 1) [Data set]. Zenodo. <http://doi.org/10.5281/zenodo.4479716>

Acknowledgements

M.D. acknowledges funding from a National Science Foundation Graduate Research Fellowship Award #1848741, H.A.G. acknowledges funding from a Rising Stars Award from the University of Texas System and a DECRA Award #DE150101981 from the Australian Research Council.

References

- Aeschbach-Hertig, W., & Gleeson, T. (2012). Regional strategies for the accelerating global problem of groundwater depletion. *Nat. Geosci.*, 5 (12), 853-861.
- Beck, H. E., et al (2019a). MSWEP V2 global 3-hourly 0.1 precipitation: methodology and quantitative assessment. *Bull. Am. Meteorol. Soc.* 100.3, 473-500.
- Beck, H. E. et al. (2019b). Daily evaluation of 26 precipitation datasets using Stage-IV gauge-radar data for the CONUS. *Hydrol. and Earth Syst. Sci.*, 23(1), 207-224.
- Bruijnzeel, L. A. (2004). Hydrological functions of tropical forests: not seeing the soil for the trees? *Agric. Ecosyst. Environ.*, 104(1), 185-228.
- Budyko, M. I. (1974). *Climate and life*. New York: Academic Press.
- Burrough, P. A. et al. *Principles of Geographical Information Systems*. (Oxford university press, New York, 2015).
- Buytaert, W. et al. (2011). Potential impacts of climate change on the environmental services of humid tropical alpine regions. *Glob. Ecol. and Biogeogr.*, 20(1), 19-33.
- Chapin, F. S. et al. (2005). Role of land-surface changes in Arctic summer warming. *Science*, 310, 657–660.
- Clark, D. A. et al. (2003). Tropical rain forest tree growth and atmospheric carbon dynamics linked to interannual temperature variation during 1984–2000. *Proceedings of the national academy of sciences*, 100(10), 5852-5857.
- Cook, B. I. et al. (2014). Global warming and 21st century drying. *Clim. Dyn.*, 43(9-10), 2607-2627.
- Creed, I. et al. (2014). Changing forest water yields in response to climate warming: Results from long-term experimental watershed sites across North America. *Glob. Chang. Biol.*, 20 (10), 3191-3208.
- Crowther, T. et al. (2015) Mapping tree-density at global scale. *Nature*. 525,201-205.
- Davidson, E. et al. (2012). The Amazon basin in transition. *Nature* 481, 321–328.
- Deb, J. C. et al. (2018). Climate change impacts on tropical forests: identifying risks for tropical Asia. *J. Trop. For. Sci.*, 30(2), 182-194.
- Dyer, E. L. et al. (2017). Congo Basin precipitation: Assessing seasonality, regional interactions, and sources of moisture. *J. Geophys. Res. Atmos.*, 122(13), 6882-6898.
- Easterling, D.R. et al. Precipitation change in the United States. in: *Climate Science Special Report: Fourth National Climate Assessment, Volume I* (eds. Wuebbles, D.J., D.W. Fahey, K.A.

Hibbard, D.J. Dokken, B.C. Stewart, and T.K. Maycock) 207-230 (U.S. Global Change Research Program, Washington, D.C., 2017).

Ellison, D.N. et al. (2012). On the forest cover–water yield debate: from demand-to supply-side thinking. *Glob. Change Biol.*, 18(3), 806-820.

Gao, G. et al. (2016). Determining the hydrological responses to climate variability and land use/cover change in the Loess Plateau with the Budyko framework. *Sci. Total Environ.*, 557, 331-342.

Giorgi, F. et al. (2011). Higher hydroclimatic intensity with global warming. *J.Clim.* 24(20), 5309-5324.

Gorelick, N. et al. (2017). Google Earth Engine: planetary-scale geospatial analysis for everyone. *Remote Sens. Environ.* 202, 18–27.

Greve, P. et al. (2016). A two-parameter Budyko function to represent conditions under which evapotranspiration exceeds precipitation. *Hydrol. Earth Syst. Sci.*, 20(6), 2195-2205.

Gudmundsson, L. et al. (2016). The sensitivity of water availability to changes in the aridity index and other factors—A probabilistic analysis in the Budyko space, *Geophys. Res. Lett.*, 43, 6985–6994.

Gutiérrez-Jurado, H. A. et al. (2006). Ecohydrology of root zone water fluxes and soil development in complex semiarid rangelands. *Hydrol. Process.*, 20(15), 3289-3316.

Gutiérrez-Jurado, H.A., et al. (2007). Ecohydrological response to a geomorphically significant flood event in a semiarid catchment with contrasting ecosystems. *Geophys.Res.Lett.*, 34(24).

Gutiérrez-Jurado. et al. (2013). On the observed ecohydrologic dynamics of a semiarid basin with aspect-delimited ecosystems. *Water Resour. Res.*, 49(12), 8263-8284.

Hartmann, D. L. et al. Observations: Atmosphere and Surface. in *Climate change 2013 The Physical Science Basis: Working Group I Contribution to the Fifth Assessment Report of the Intergovernmental Panel on Climate Change: Volume 9781107057999* 159-254 (Cambridge University Press, Cambridge, 2013).

Held, I. M., & Soden, B. J. (2006). Robust responses of the hydrological cycle to global warming. *J. Clim.*, 19(21), 5686-5699.

Helman, D., et al. (2017). Forests growing under dry conditions have higher hydrological resilience to drought than do more humid forests. *Glob. Change Biol.*, 23(7), 2801-2817.

Hinzman, L. D. et al. (2013). Trajectory of the Arctic as an integrated system. *Ecol. Appl.*, 23(8), 1837-1868.

Huntington, T. G. (2006). Evidence for intensification of the global water cycle: review and synthesis. *J. Hydrol.*, 319(1-4), 83-95.

- Jarvis, A. et al. (2008). Hole-filled SRTM for the Globe Version 4. *available from the CGIAR-CSI SRTM 90m Database (<http://srtm.csi.cgiar.org>)*, 15, 25-54
- Lamprecht, A. et al. (2018). Climate change leads to accelerated transformation of high-elevation vegetation in the central Alps. *New Phytol.*, 220(2), 447-459.
- Lenton, T. M. et al. (2008). Tipping elements in the Earth's climate system. *Proc. Natl Acad. Sci.*, 105(6), 1786-1793.
- Li, C. et al. (2019). Larger increases in more extreme local precipitation events as climate warms. *Geophys. Res. Lett.*, 46(12), 6885-6891.
- López-Moreno, J. I., et al. (2010). Decoupling of warming mountain snowpacks from hydrological regimes. *Environ. Res. Lett.*, 15(11), 114006.
- Martens, B. et al. (2018). Terrestrial evaporation response to modes of climate variability. *NPJ Clim. Atmos. Science*, 1(1), 1-7.
- Milly, P. C. et al. (2005). Global pattern of trends in streamflow and water availability in a changing climate. *Nature*, 438(7066), 347-350.
- Motew, M. M., & Kucharik, C. J. (2013). Climate-induced changes in biome distribution, NPP, and hydrology in the Upper Midwest US: A case study for potential vegetation. *J. Geophys. Res. Biogeosci.*, 118(1), 248-264.
- Myers-Smith, I. H. et al. (2015). Climate sensitivity of shrub growth across the tundra biome. *Nat. Clim. Change*, 5(9), 887-891.
- Najafi, M. R. et al. (2015). Attribution of Arctic temperature change to greenhouse-gas and aerosol influences. *Nat. Clim. Change*, 5(3), 246-249.
- Ohmura, A. (2012). Enhanced temperature variability in high-altitude climate change. *Theor. Appl. Climatol.*, 110(4), 499-508.
- Olson, D. M. et al. (2001). Terrestrial ecoregions of the world: a new map of life on Earth. *Bioscience* 51(11):933-938.
- Palazzi, E., et al. (2019). Elevation-dependent warming in global climate model simulations at high spatial resolution. *Clim. Dyn.*, 52(5-6), 2685-2702
- Padron, R. S., et al. (2017). Large Scale controls of the surface water balance over land: Insights from a systematic review and meta-analysis. *Wat. Resour. Res.*, 53, 9659– 9678.
- Pecl, G. T. et al. (2017). Biodiversity redistribution under climate change: Impacts on ecosystems and human well-being. *Science*, 355(6332).
- Pepin, N. et al. (2015). Elevation-dependent warming in mountainous regions of the world. *Nat. Clim. Change*, 5, 424-430.

- Reyer, C.P. et al. (2017). Climate change impacts in Latin America and the Caribbean and their implications for development. *Reg. Environ. Change*, 17.6, 1601-1621.
- Riebe, C. S. et al. (2015). Climate and topography control the size and flux of sediment produced on steep mountain slopes. *Proc. Natl. Acad. Sci.*, 112(51), 15574-15579.
- Risser, M. D., & Wehner, M. F. (2017). Attributable human-induced changes in the likelihood and magnitude of the observed extreme precipitation during Hurricane Harvey. *Geophys. Res. Lett.*, 44.
- Rodell, M. et al. (2018). Emerging Trends in Global Freshwater. *Nature*, 557, 651–659.
- Roderick, M. L., F. et al. (2014). A general framework for understanding the response of the water cycle to global warming over land and ocean, *Hydrol. Earth Syst. Sci.*, 18(5), 1575–1589.
- Roudier, P. et al. (2014). Climate change impacts on runoff in West Africa: a review. *Hydrol. Earth Syst. Sci.*, 18, 2789-3801.
- Running, S. et al. (2017). MOD16A2 MODIS/Terra Net Evapotranspiration 8-Day L4 Global 500 m SIN Grid V006. NASA EOSDIS Land Processes DAAC.
- Salmoral, G. et al. (2015). Drivers influencing streamflow changes in the Upper Turia basin, Spain. *Sci. Total Environ.*, 503, 258-268.
- Seddon, A.W.R. et al. (2016). Sensitivity of Global Terrestrial Ecosystems to Climate Variability, *Nature*, 531, 229–232.
- Siler, N. et al. (2018). Insights into the zonal-mean response of the hydrologic cycle to global warming from a diffusive energy balance model. *J. Clim.*, 31(18), 7481-7493.
- Sinha, J. et al. (2018). Assessment of the impacts of climatic variability and anthropogenic stress on hydrologic resilience to warming shifts in Peninsular India. *Sci. Rep.*, 8(1), 1-14.
- Staal, A. et al. (2018). Forest-rainfall cascades buffer against drought across Amazon. *Nat. Clim. Change.*, 8, 539–543.
- Sterling, S. M. et al. (2013). The impact of global land-cover change on the terrestrial water cycle. *Nat. Clim. Change*, 3(4), 385.
- Srivastava, A. et al. (2020). The Role of Landscape Morphology on Soil Moisture Variability in Semi-arid Ecosystems. *Hydrol. Process.*
- Stott, P. (2016). How climate change affects extreme weather events. *Science*, 352(6293), 1517-1518
- Tabari, H. (2020). Climate change impact on flood and extreme precipitation increases with water availability. *Sci. Rep.*, 10(1), 1-10

- Trenberth, K. E. (2011). Changes in precipitation with climate change. *Clim. Res.*, 47(1-2), 123-138.
- Uuh-Sonda, J. M., Gutiérrez-Jurado, H. A., Figueroa-Espinoza, B., & Méndez-Barroso, L. A. (2018). On the ecohydrology of the Yucatan Peninsula: Evapotranspiration and carbon intake dynamics across an eco-climatic gradient. *Hydrol. Proc.*, 32(18), 2806–2828. <https://doi.org/10.1002/hyp.13230>
- van der Ent, R. J. et al. (2010). Origin and fate of atmospheric moisture over continents. *Wat. Resour. Res.*, 46(9).
- van Oldenborgh, G. J. et al. (2017). Attribution of extreme rainfall from Hurricane Harvey, August 2017. *Environ. Res. Lett.*, 12(12), 124009.
- Wu, J., Miao, C., Zhang, X., Yang, T., & Duan, Q. (2017a). Detecting the quantitative hydrological response to changes in climate and human activities. *Science of the Total Environment*, 586, 328-337.
- Wu, J. et al. (2017b). Contribution analysis of the long-term changes in seasonal runoff on the Loess Plateau, China, using eight Budyko-based methods. *J. Hydrol.*, 545, 263-275.
- Wu, T. et al. (2019). Warming effects on leaf nutrients and plant growth in tropical forests. *Plant Ecol.*, 220(7-8), 663-674.
- Yan, L., et al. (2016). Mechanisms of elevation-dependent warming over the Tibetan plateau in quadrupled CO₂ experiments. *Clim. Change*, 135(3-4), 509-519.
- Yeh, P. J. F., & Wu, C. (2018). Recent acceleration of the terrestrial hydrologic cycle in the US Midwest. *J. Geophys. Res. Atmos.*, 123(6), 2993-3008.
- Zhan, C. et al. (2012). Hydrologic response to climate variability and human activities in the Chao River catchment near Beijing. *Water Int.*, 37(5), 585-597.
- Zhang, X. et al. (2013). Enhanced poleward moisture transport and amplified northern high-latitude wetting trend. *Nat. Clim. Change*, 3(1), 47-51.
- Zhang, Y. et al. (2019). Coupled estimation of 500 m and 8-day resolution global evapotranspiration and gross primary production in 2002–2017. *Remote Sens. of Environ.*, 222, 165-182.
- Zhang, G. et al. (2020). Response of Tibetan Plateau lakes to climate change: Trends, patterns, and mechanisms. *Earth-Science Reviews*, 208, 1-22. doi.org/10.1016/j.earscirev.2020.103269
- Zhou, X. et al. (2013). An imperative need for global change research in tropical forests. *Tree Physiol.*, 33(9), 903-912.

Vita

Marisol Dominguez Tuda completed her B.Sc. in Environmental Sciences degree at the University of Texas at El Paso (UTEP) in Spring 2016. She then enrolled in the PhD in Geology (Hydrology focus) in the Spring of 2017 at UTEP. She has decided to graduate from her master's degree in summer 2021. Marisol continues to pursue a Ph.D. in Geological Sciences at the same university and is expected to graduate in 2023. As an undergraduate student, she worked as a Math Tutor and volunteered as an intern at the Environmental Protection Agency (EPA) Region 6. Throughout her time as a graduate student, she worked as a research assistant and presented her research at multiple conferences such as the American Geophysical Union (AGU, 2017, 2018) and European Geophysical Union (EGU, 2019), Japan Geophysical Union (JPGU, 2019). In the Spring of 2018, Marisol was granted the National Science Foundation Graduate Fellowship to fund her research. In Fall 2018, she won the Outstanding Paper Award at the AGU Conference. In March of 2019, she won 2nd place for a 3-Minute Thesis Competition held at her university. Apart from her science career, she is a professional painter which focuses in painting wildlife. Lastly, she is currently working on publishing her work entitled "Global Analysis of the Hydrologic Sensitivity to Climate Variability."

Contact Information: mdominguez31@miners.utep.edu

Website: <https://www.marisoldomingueztuda.com>

This thesis was typed by Marisol Dominguez Tuda